

Scheme 2 Selected examples of compounds discussed in this study. $[\text{Ir}(\text{PCy}_3)_2(\text{H})_2(\eta^2\text{-H}_3\text{B}\cdot(\text{NRHBH}_2)_n\cdot\text{NRH}_2)][\text{BAR}^{\text{F}}_4]$, R = Me, 5; H, 6; $n = 0$, a; $n = 1$, b; $n = 2$, c; $n = 3$, d; $n = 4$, e. $[\text{BAR}^{\text{F}}_4]^-$ anions are not shown. * = corresponding amino-borane.

and $\text{H}_3\text{B}\cdot\text{NMe}_2\text{H}$ and the previously noted requirement for additional amine-borane to promote this process.²¹

Results and discussion

Addition of one equivalent of $\text{H}_3\text{B}\cdot\text{NH}_3$ to **1**¹⁹ in $\text{C}_6\text{H}_5\text{F}$ solvent results in the immediate formation of the sigma amine-borane complex $[\text{Ir}(\text{PCy}_3)_2(\text{H})_2(\eta^2\text{-H}_3\text{B}\cdot\text{NH}_3)][\text{BAR}^{\text{F}}_4]$ **6a** in quantitative yield by NMR spectroscopy. There is no onward dehydrogenation after 4 hours under these conditions, but addition of further $\text{H}_3\text{B}\cdot\text{NH}_3$ (10 equivalents total) results in the formation of higher oligomers, $[\text{Ir}(\text{PCy}_3)_2(\text{H})_2\{\eta^2\text{-H}_3\text{B}\cdot(\text{NH}_2\text{BH}_2)_n\cdot\text{NH}_3\}][\text{BAR}^{\text{F}}_4]$ $n = 1-4$. This requirement for additional amine-borane to promote dehydrogenation has been noted before in these systems, although its role has only been speculated upon.²¹ Fig. 1 shows the ESI-MS spectra of the reaction of **1** with the amine-boranes $\text{H}_3\text{B}\cdot\text{NMe}_x\text{H}_{3-x}$ ($x = 0-3$) demonstrating the increasing degrees of dehydrogenation and oligomerisation with decreasing steric bulk of the amine-borane. Under these conditions $\text{H}_3\text{B}\cdot\text{NMe}_2\text{H}$ undergoes dehydrogenation with no subsequent B-N coupling (**4a***),¹⁹ while $\text{H}_3\text{B}\cdot\text{NMeH}_2$ gives the product of one dehydrocoupling event (**5b**).²¹ By contrast for $\text{H}_3\text{B}\cdot\text{NH}_3$ metal-bound oligomers arising from up to four of these dehydrocoupling events are observed by ESI-MS (**6b-e**), which all show excellent fits with calculated isotopomer patterns, with **6d/e** ($n = 4, 5$; Scheme 2) observed as $[\text{M}-\text{H}_2]^+$ cations. In the $^1\text{H}\{^1\text{B}\}$ NMR spectrum of this mixture three distinct pairs of Ir...H-B and Ir-H environments are observed in an approximate 1 : 10 : 10 ratio (see ESI†), which are assigned to **6a**, **6b** and **6c** respectively (*vide infra*), consistent with the major species observed by ESI-MS (**6a-c**). The $^{11}\text{B}\{^1\text{H}\}$ NMR spectrum of this mixture shows broad, potentially overlapping, signals in the Ir...H₃B and {BH₂} regions, and the $^{31}\text{P}\{^1\text{H}\}$ NMR spectrum shows two tightly-coupled AB doublets in approximately equal ratio, the third species (*i.e.* **6a**) being too low in intensity to be observed. The identity of these complexes has been confirmed by the independent synthesis of **6b** and **6c** from the preformed

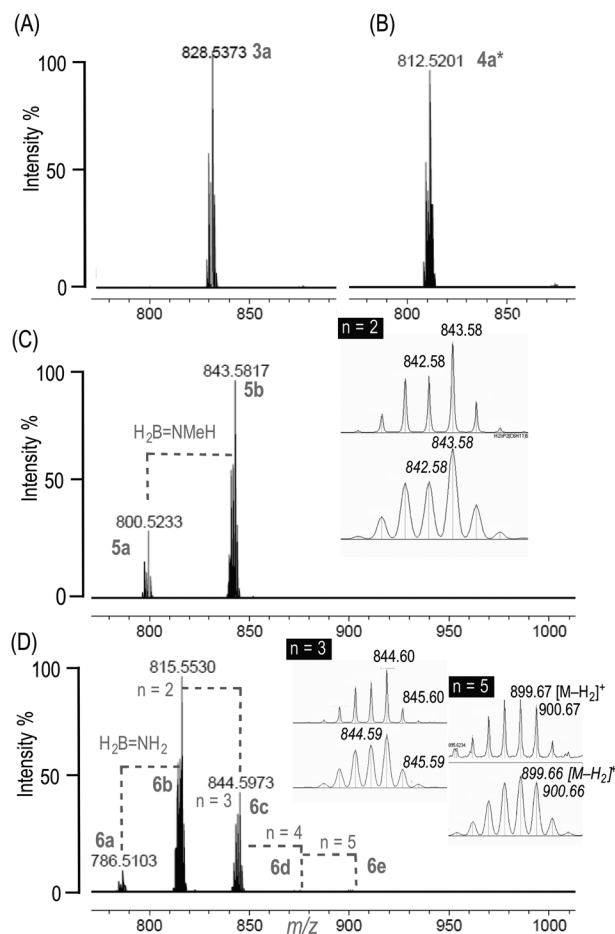
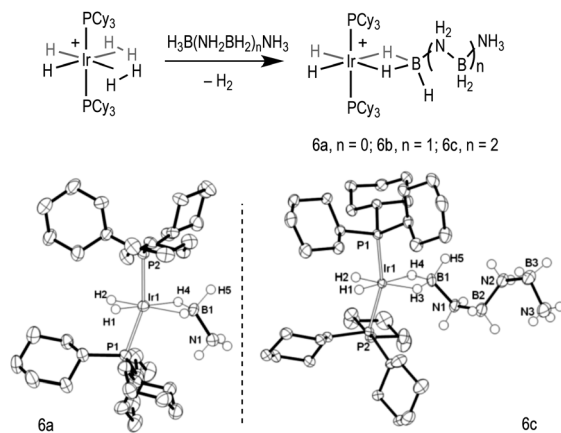


Fig. 1 ESI-MS (positive mode) of **1** ($\text{C}_6\text{H}_5\text{F}$ solution) and 10 equivalents of: (A) $\text{H}_3\text{B}\cdot\text{NMe}_3$, **3a**; (B) $\text{H}_3\text{B}\cdot\text{NMe}_2\text{H}$, **4a*** (96 h, 3 equiv.); (C) $\text{H}_3\text{B}\cdot\text{NMeH}_2$, **5a/5b** (D) $\text{H}_3\text{B}\cdot\text{NH}_3$, **6a-e**; Calculated isotopomer m/z given in italics; $n = 4$ obs. $m/z = 871.63$ $[\text{M} - \text{H}_2]^+$, calc. 871.62. After 4 hours unless otherwise stated. See Scheme 2 for numbering, and ESI† for an expansion of (D).

borazanes $\text{H}_3\text{B}\cdot\text{NH}_2\text{BH}_2\cdot\text{NH}_3$ ²⁸ and $\text{H}_3\text{B}\cdot(\text{NH}_2\text{BH}_2)_2\cdot\text{NH}_3$ ²⁹ respectively. Scheme 3 shows the solid-state structure (as the $[\text{BAR}^{\text{Cl}}_4]^-$ salts³⁰ from $[\text{Ir}(\text{PCy}_3)_2(\text{H})_2(\text{H}_2)_2][\text{BAR}^{\text{Cl}}_4]$, **2**) of **6c**, alongside that of **6a**, which confirm formulation, being closely related to analogous complexes **3a**, **4a**, **5a** and **5b**.^{19,21} Over time (24 h) these mixtures of products degrade to give bimetallic products identified by ESI-MS as $[\{\text{Ir}(\text{PCy}_3)_2(\text{H})_2\}_2\{\text{H}_3\text{B}(\text{NH}_2\text{BH}_2)_n\text{H}\}]^+$ **7a-d** ($n = 0$ to 3 respectively), presumably in which the anionic amino-boranes $[\text{H}_3\text{B}(\text{NH}_2\text{BH}_2)_n\text{H}]^-$ ²⁹ bridge between two cationic metal fragments. Recrystallisation of this mixture afforded small amounts of the borohydride complex³¹ $[\{\text{Ir}(\text{PCy}_3)_2(\text{H})_2\}_2(\eta^2, \eta^2\text{-H}_2\text{BH}_2)][\text{BAR}^{\text{F}}_4]$ **7a** (see ESI† for a solid-state structure). We were unable to definitely characterise the other byproducts of this decomposition.

Borazine was also observed during the oligomerisation of $\text{H}_3\text{B}\cdot\text{NH}_3$ (~10% by ^{11}B NMR spectroscopy relative to $[\text{BAR}^{\text{F}}_4]^-$), which might suggest free amino-borane is formed as a transient intermediate during the reaction.^{15,18} Addition of excess cyclohexene to the reaction did not result in the observation of any hydroboration product, $\text{Cy}_2\text{B}=\text{NH}_2$, a trapping reaction that

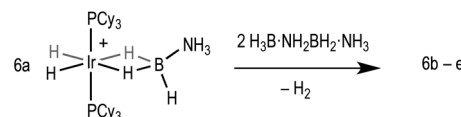




Scheme 3 Synthesis of **6a**, **6b** and **6c**. Solid-state structures (50% displacement ellipsoids) of **6a** and **6c**. Selected hydrogen atoms are shown and the $[\text{BAr}^{\text{Cl}}_4]^-$ anions are omitted for clarity. See ESI† for full details.

has previously been suggested to be indicative of free amino-borane in dehydrocoupling reactions.¹⁵ As recently noted, however, this process relies on hydroboration being kinetically competitive with oligomerisation, which might not necessarily be the case.¹⁰

Although these data are consistent with a growing oligomeric chain at the $\{\text{Ir}(\text{PCy}_3)_2(\text{H})_2\}^+$ fragment, similar to those observed by ESI-MS for olefin polymerisation,^{32,33} these observations cannot discount a scenario where metal-catalysed dehydrogenation forms the free amino-borane, $\text{H}_2\text{B}=\text{NH}_2$, which then polymerises off-metal,¹³ with the most soluble short-chain oligomers then coordinating to the metal fragment. However, as computation suggests (*vide infra*) that the first dehydrogenation has a significantly higher barrier than subsequent oligomerisation we propose that this scenario is less likely. To probe further the oligomerisation process, three sequential additions of 1.1 equivalents of $\text{H}_3\text{B}\cdot\text{NH}_3$ to **1** gave progressively longer oligomer chains (*i.e.* **6a–6c**) as measured by ESI-MS (see ESI†), although this mixture was biased towards **6a** and **6b**, suggesting that the sigma-bound oligomeric units, *e.g.* **6b** or **6c**, are only weakly bound with the metal centre and can be displaced by excess $\text{H}_3\text{B}\cdot\text{NH}_3$. Confirming this, addition of two equivalents of $\text{H}_3\text{B}\cdot\text{NH}_3$ to **6c** immediately results in a mixture of **6a–c** and free $\text{H}_3\text{B}\cdot(\text{NH}_2\text{BH}_2)_2\cdot\text{NH}_3$, with **6c** the major observed product. After 4 hours this has developed into a mixture of **6a–e** with **6b** and **6c** the major products. Addition of 2 equivalents of $\text{H}_3\text{B}\cdot\text{NH}_2\text{BH}_2\cdot\text{NH}_3$ to **6a** results in the formation of **6b** and relatively smaller amounts of **6c–6e** (by ESI-MS), the latter presumably derived from further dehydrocoupling events from **6b** with $\text{H}_3\text{B}\cdot\text{NH}_3$ (Scheme 4). Overall this suggests a mechanism in which the formed sigma-bound oligomer can be displaced by other amine-boranes, *i.e.* reversible chain transfer can occur. At the end of the reaction (24 h) a white solid is recovered that shows an IR spectrum essentially identical to polyaminoborane.³⁴ Use of 5 equivalents each of $\text{H}_3\text{B}\cdot\text{NH}_3$ and $\text{H}_3\text{B}\cdot\text{NMe}_2$ gave a mixture of metal-bound co-oligomers $[\text{Ir}(\text{PCy}_3)_2(\text{H})_2\{\text{H}(\text{H}_2\text{BNH}_2)_x(\text{H}_2\text{BNMeH})_y\}]^+$ ($x = 0, 1, y = 1, 2; x = 1, y = 0; x = 2, y = 1$).



Scheme 4 Addition of 2 equivalents of $\text{H}_3\text{B}\cdot(\text{NH}_2\text{BH}_2)\cdot\text{NH}_3$ to **6a** results in the formation of higher oligomers.

Density functional theory (DFT) calculations³⁵ have been used to study the mechanism of the dehydrocoupling of $\text{H}_3\text{B}\cdot\text{NH}_3$ at **6a** with particular focus on (i) the requirement for additional $\text{H}_3\text{B}\cdot\text{NH}_3$ to induce dehydrogenation, (ii) the mechanism of the B–N coupling step and (iii) the varying affinities of the different amine-boranes toward oligomerisation. These calculations employed PMe_3 ligands, with $[\text{Ir}(\text{PMe}_3)_2(\text{H})_2(\eta^2\text{-H}_3\text{B}\cdot\text{NMe}_x\text{H}_{3-x})]^+$ (denoted **6a'**, $x = 0$, **5a'**, $x = 1$ and **4a'**, $x = 2$) the model initial reactants, and use a BP86-D3($\text{C}_6\text{H}_5\text{F}$) protocol. We report free energies derived from gas-phase BP86-optimisations, corrected for dispersion and solvation effects. Each key step in the dehydrocoupling process (B–H/N–H bond activation and B–N bond coupling) presented more than one possible transition state and the most accessible of these are presented here, with alternative structures given in the ESI.†

We have previously modelled the dehydrogenation of $\text{H}_3\text{B}\cdot\text{NMe}_2\text{H}$ in $[\text{Ir}(\text{PMe}_3)_2(\text{H})_2(\eta^2\text{-H}_3\text{B}\cdot\text{NMe}_2\text{H})]^+$ (**4a'**) to form the corresponding amino-borane adduct (*i.e.* **4a'***, a model of **4a*** in Scheme 2) and defined a mechanism based on sequential B–H activation, H_2 loss and rate-limiting N–H activation.¹⁹ Applying this mechanism to $\text{H}_3\text{B}\cdot\text{NH}_3$ dehydrogenation in **6a'** reveals a barrier of $33.8 \text{ kcal mol}^{-1}$ in which the N–H activation step is again rate-limiting (see Fig. S1–3, ESI†). With an added $\text{H}_3\text{B}\cdot\text{NH}_3$ molecule a related mechanism can be characterised but with a significantly reduced barrier of $26.7 \text{ kcal mol}^{-1}$ (Fig. 2). In this process the second $\text{H}_3\text{B}\cdot\text{NH}_3$ molecule first adds to **6a'** to give $[\text{Ir}(\text{PMe}_3)_2(\text{H})_2(\eta^1\text{-H}_3\text{B}\cdot\text{NH}_3)_2]^+$, **16a'_1**, with a binding energy of $5.0 \text{ kcal mol}^{-1}$. This stabilisation is in part due to a $\text{BH}(\delta^-)\cdots\text{H}(\delta^+)\text{N}$ dihydrogen interaction between the two $\text{H}_3\text{B}\cdot\text{NH}_3$ ligands.^{36,37} B–H activation in **16a'_1** entails a

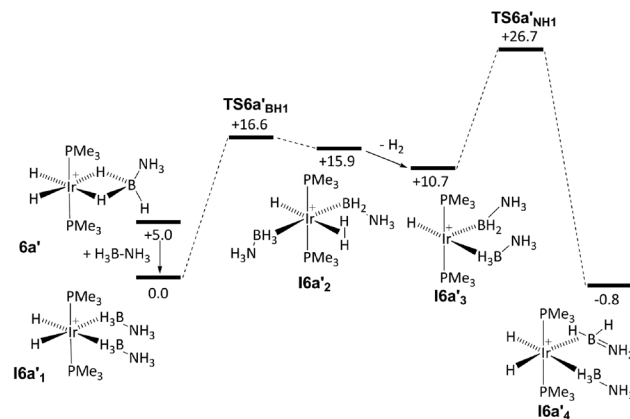


Fig. 2 Computed free energy reaction profile (kcal mol^{-1} , BP86-D3($\text{C}_6\text{H}_5\text{F}$)) for dehydrogenation of $\text{H}_3\text{B}\cdot\text{NH}_3$ in **6a'** in the presence of added $\text{H}_3\text{B}\cdot\text{NH}_3$.



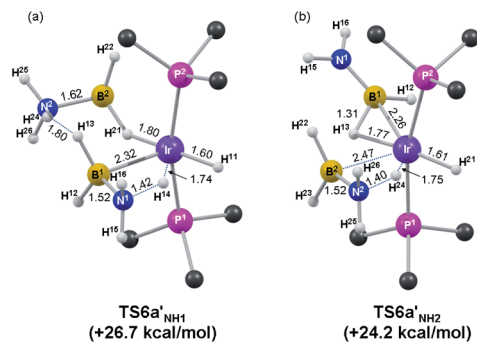


Fig. 3 Computed structures of the rate-limiting N–H activation transition states of (a) a first and (b) a second $\text{H}_3\text{B}\cdot\text{NH}_3$ molecule at $\mathbf{6a}'$. Key distances are in Å and PMe_3 H atoms are omitted for clarity.

barrier of $16.6 \text{ kcal mol}^{-1}$ via $\text{TS6a}'_{\text{BH1}}$ and proceeds with concomitant reductive coupling of the two hydride ligands to give $[\text{Ir}(\text{PMe}_3)_2(\text{BH}_2\text{NH}_3)(\text{H})(\text{H}_2)(\eta^1\text{-H}_3\text{B}\cdot\text{NH}_3)]^+$, $\mathbf{I6a}'_2$ ($G = +15.9 \text{ kcal mol}^{-1}$). H_2 loss then leads to $\mathbf{I6a}'_3$ ($G = +10.7 \text{ kcal mol}^{-1}$) from which rate-limiting N–H activation occurs via $\text{TS6a}'_{\text{NH1}}$ ($G = +26.7 \text{ kcal mol}^{-1}$) to give $\mathbf{I6a}'_4$ in which both an amine- and an amino-borane are bound to the metal centre.

The computed geometry of $\text{TS6a}'_{\text{NH1}}$ is shown in Fig. 3a and shows transfer of H^{14} from the BH_2NH_3 ligand to Ir ($\text{N}^1\cdots\text{H}^{14} = 1.42 \text{ Å}$; $\text{Ir}\cdots\text{H}^{14} = 1.74 \text{ Å}$) while a dihydrogen bonding interaction is maintained with the spectator $\text{H}_3\text{B}\cdot\text{NH}_3$ ligand ($\text{H}^{24}\cdots\text{H}^{13} = 1.80 \text{ Å}$). This feature stabilises both $\text{TS6a}'_{\text{NH1}}$ and its precursor $\mathbf{I6a}'_3$ and so contributes to a reduction in the overall barrier to dehydrogenation of $7.1 \text{ kcal mol}^{-1}$ compared to the reaction direct from $\mathbf{6a}'$ without added amine-borane. An alternative transition state, $\text{TS6a}'_{\text{NH1}}(\text{Alt } \mathbf{1})$, in which the second $\text{H}_3\text{B}\cdot\text{NH}_3$ ligand adopts an $\eta^2\text{-(B,H)}$ bonding mode (similar to the amino-borane ligand in $\text{TS6a}'_{\text{NH2}}$, see Fig. 3b and below) is comparable in energy ($G = +26.9 \text{ kcal mol}^{-1}$, see Fig. S6(b)†). Both forms of $\text{TS6a}'_{\text{NH1}}$ are consistent with dehydrogenation being facilitated by the addition of amine-borane to $\mathbf{6a}'$. Similar reductions in barriers to dehydrogenation have very recently been reported for $\text{H}_3\text{B}\cdot\text{NMe}_2\text{H}$ dehydrogenation using $\{\text{Rh}(\text{chelating phosphine})\}^+$ fragments.³⁸

For the subsequent B–N coupling step a total seven different pathways have been characterised. Four of these stem from intermediate $\mathbf{I6a}'_4$ and entail B–H activation in the $\text{H}_3\text{B}\cdot\text{NH}_3$ ligand to produce a Lewis acidic $\{\text{H}_2\text{BNH}_3\}$ moiety that then couples with $\text{H}_2\text{B}=\text{NH}_2$. In most cases these processes occur in one step. Two further pathways have been characterised for the direct reaction of free $\text{H}_2\text{B}=\text{NH}_2$ with either $\mathbf{6a}'$ or its B–H activated form. All of these pathways, however, have computed barriers in excess of 28 kcal mol^{-1} , and as this is higher than the barrier to dehydrogenation these pathways would be inconsistent with the lack of any bound amino-borane intermediates being observed experimentally. Full details of these alternative pathways are given in the ESI (see Fig. S12†).

A significantly more accessible B–N coupling route was characterised that involved the direct reaction of two $\text{H}_2\text{B}=\text{NH}_2$ units. This process therefore requires the prior dehydrogenation

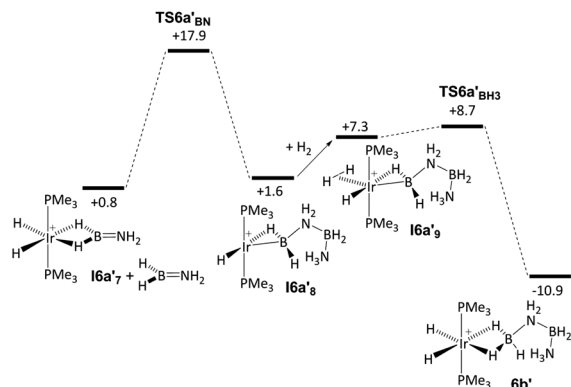


Fig. 4 Computed free energy reaction profile (kcal mol^{-1} , BP86-D3($\text{C}_6\text{H}_5\text{F}$)) for B–N coupling and formation of oligomerisation product $\mathbf{6b}'$.

of a second $\text{H}_3\text{B}\cdot\text{NH}_3$ molecule and a pathway for this, analogous to that shown in Fig. 2, has been defined starting from $\mathbf{I6a}'_4$ and forming $[\text{Ir}(\text{PMe}_3)_2(\text{H}_2)(\eta^2\text{-H}_2\text{B}=\text{NH}_2)]^+$ ($\mathbf{I6a}'_7$) and free $\text{H}_2\text{B}=\text{NH}_2$ (see also Fig. S7–9†). $\mathbf{I6a}'_7$ is closely related to that calculated for the product of dehydrogenation of $\text{H}_3\text{B}\cdot\text{NMe}_2\text{H}$ by the same fragment.¹⁹ The key N–H activation transition state in this process, $\text{TS6a}'_{\text{NH2}}$ (Fig. 3b), has a free energy of $+24.2 \text{ kcal mol}^{-1}$ and features a spectator $\eta^2\text{-(B,H)-H}_2\text{B}=\text{NH}_2$ ligand³⁹ that stabilises the metal centre. Oligomerisation then proceeds through the reaction of $\mathbf{I6a}'_7$ with $\text{H}_2\text{B}=\text{NH}_2$ and the associated reaction profile (Fig. 4) shows B–N coupling via $\text{TS6a}'_{\text{BN}}$ at only $+17.9 \text{ kcal mol}^{-1}$. The structure of this transition state (Fig. 5) shows that the Ir-bound amino-borane has rearranged to an $\eta^2\text{-(B,H)}$ mode that exposes the pendant $\{\text{NH}_2\}$ moiety to attack by the second, incoming amino-borane ($\text{N}^1\cdots\text{B}^2 = 2.37 \text{ Å}$). As this occurs a hydride transfers from Ir onto N^2 ($\text{Ir}\cdots\text{H}^{24} = 1.63 \text{ Å}$; $\text{H}^{24}\cdots\text{N}^2 = 1.64 \text{ Å}$) to generate an $\eta^2\text{-(B,H)-H}_2\text{B}\cdot\text{NH}_2\text{BH}_2\cdot\text{NH}_3$ ligand in the resultant intermediate $\mathbf{I6a}'_8$ ($G = +1.6 \text{ kcal mol}^{-1}$). Addition of H_2 ($\mathbf{I6a}'_9$, $G = +7.3 \text{ kcal mol}^{-1}$) and facile B–H reductive coupling gives the final model product, $[\text{Ir}(\text{PMe}_3)_2(\text{H})_2(\eta^2\text{-H}_3\text{B}\cdot\text{NH}_2\text{BH}_2\cdot\text{NH}_3)]^+$, $\mathbf{6b}'$ ($G = -10.9 \text{ kcal mol}^{-1}$).⁴⁰ This coupling process is similar to that suggested by

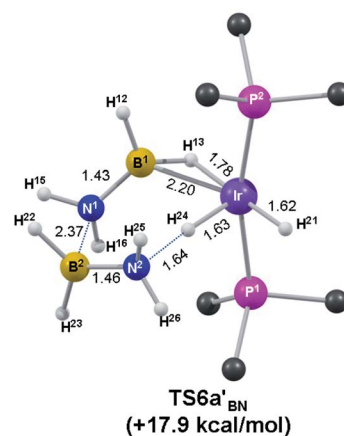


Fig. 5 Computed B–N coupling transition state with key distances in Å and PMe_3 H atoms omitted for clarity.



Schneider and co-workers in bifunctional $\text{Ru}(\text{H})_2(\text{PMe}_3)(\text{PNP})$ catalysis [$\text{PNP} = \text{HN}(\text{CH}_2\text{CH}_2\text{P}^t\text{Bu}_2)_2$], in which an N–H activated $\text{H}_3\text{B}\cdot\text{NH}_3$ group undergoes B–N coupling with $\text{H}_2\text{B}=\text{NH}_2$ during dehydropolymerisation.¹⁰

Reaction profiles analogous to those in Fig. 2 and 4 were also computed for the dehydrocoupling of $\text{H}_3\text{B}\cdot\text{NMe}_2$ at **5a'** and $\text{H}_3\text{B}\cdot\text{NMe}_2\text{H}$ at **4a'**. Similar dehydrogenation barriers are found in each case (**5a'**/ $\text{H}_3\text{B}\cdot\text{NMe}_2$: 25.2 kcal mol⁻¹; **4a'**/ $\text{H}_3\text{B}\cdot\text{NMe}_2\text{H}$: 26.2 kcal mol⁻¹) and in the absence of a second amine-borane molecule these barriers increase to above 33 kcal mol⁻¹, reiterating the promotional effect of added amine-borane on this process. In contrast the B–N coupling transition states are more substrate-dependent and increase significantly in energy with the size of the amine-borane (**6a'**/ $\text{H}_3\text{B}\cdot\text{NH}_3$: 17.9 kcal mol⁻¹; **5a'**/ $\text{H}_3\text{B}\cdot\text{NMe}_2$: 19.9 kcal mol⁻¹; **4a'**/ $\text{H}_3\text{B}\cdot\text{NMe}_2\text{H}$: 26.5 kcal mol⁻¹). This trend is consistent with oligomerisation being accessible for both $\text{H}_3\text{B}\cdot\text{NH}_3$ and $\text{H}_3\text{B}\cdot\text{NMe}_2$, but this step becoming significantly more difficult for the larger $\text{H}_3\text{B}\cdot\text{NMe}_2\text{H}$. Indeed oligomerisation is not seen experimentally for **4a'**/ $\text{H}_3\text{B}\cdot\text{NMe}_2\text{H}$ under the conditions used here.⁴¹

An analogous mechanism based on dehydrocoupling of $\text{H}_3\text{B}\cdot\text{NH}_3$ and $\text{H}_3\text{B}\cdot\text{NH}_2\text{BH}_2\cdot\text{NH}_3$ can account for the formation of the $\text{H}_3\text{B}\cdot(\text{NH}_2\text{BH}_2)_2\cdot\text{NH}_3$ trimer seen in **6c** (modelled by **6c'**). The key energetics are similar to those computed in the pathway for the formation of **6b'**: dehydrogenation of $\text{H}_3\text{B}\cdot\text{NH}_3$ (in the presence of $\text{H}_3\text{B}\cdot\text{NH}_2\text{BH}_2\cdot\text{NH}_3$) has an overall barrier of 26.3 kcal mol⁻¹, then dehydrogenation of $\text{H}_3\text{B}\cdot\text{NH}_2\text{BH}_2\cdot\text{NH}_3$ (now in the presence of $\text{H}_2\text{N}=\text{BH}_2$) has a barrier of 24.3 kcal mol⁻¹. The order of dehydrogenation is important, however, as the alternative initial dehydrogenation of $\text{H}_3\text{B}\cdot\text{NH}_2\text{BH}_2\cdot\text{NH}_3$ (in the presence of $\text{H}_3\text{B}\cdot\text{NH}_3$) has a higher barrier of 28.1 kcal mol⁻¹ (see Fig. S15[†]). The subsequent B–N coupling transition state is again more accessible than dehydrogenation, **TS6b'**_{BNA} (Fig. 6a) having a computed energy of 21.2 kcal mol⁻¹. In this case there are two possible B–N coupling outcomes, depending on whether $\text{H}_2\text{B}=\text{NH}_2$ (as in **TS6b'**_{BNA}) or $\text{H}_2\text{B}=\text{NHBH}_2\cdot\text{NH}_3$ (**TS6b'**_{BNB}, Fig. 6b) is bound to Ir in the transition state. The former case leads to a straight chain oligomer product, and is 2.3 kcal mol⁻¹ more stable than the alternative that gives a branched chain product. The barrier for this second oligomerisation step is close to that for the B–N coupling of $\text{H}_3\text{B}\cdot\text{NMe}_2$ (19.9 kcal mol⁻¹), highlighting the similar behaviour of these two mono-substituted amine-boranes. This in turn suggests

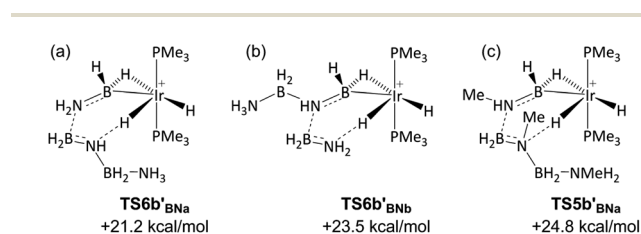
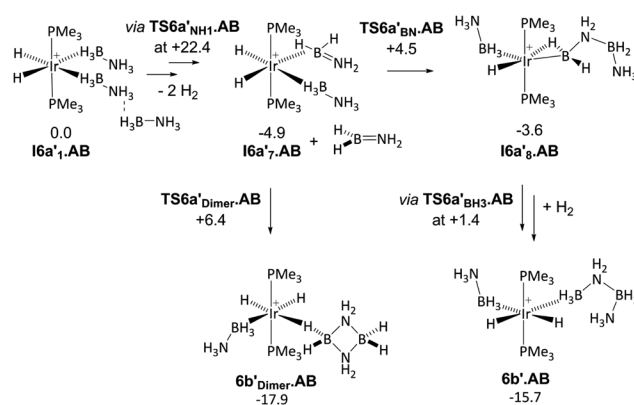


Fig. 6 Transition states for B–N bond coupling leading to (a) straight chain and (b) branched chain formation in **6c'** as well as (c) straight chain formation in **5c'**. Free energies (kcal mol⁻¹, BP86-D3(C₆H₅F)) are quoted relative to $[\text{Ir}(\text{PMe}_3)_2(\text{H})_2(\eta^2\text{-H}_3\text{B}\cdot\text{NMe}_x\text{H}_{3-x})(\eta^1\text{-H}_3\text{B}\cdot\text{NMe}_x\text{H}_{2-x}\text{BH}_2\cdot\text{NMe}_x\text{H}_{3-x})]^+$ (**I6b'**₁, $x = 0$; **I5b'**₁, $x = 1$) as appropriate.

that subsequent chain growth with further $\text{H}_3\text{B}\cdot\text{NH}_3$ may proceed *via* transition states related to **TS6b'**_{BNA} in which the growing oligomer chain extends away from the metal centre with minimal additional steric impact. By the same token, $\text{H}_3\text{B}\cdot\text{NMe}_2$ trimerisation is more difficult with the equivalent transition state, **TS5b'**_{BNA}, equating to a higher barrier of +24.8 kcal mol⁻¹ (Fig. 6c). This trend towards higher oligomerisation barriers as the size of the amine-borane increases is consistent with the experimental observations (*i.e.* **5a** giving **5b** alone whereas **6a** can undergo multiple oligomerisation steps to give **6b–e**).

A potential side reaction within this mechanistic picture involves the cyclisation of two aminoborane fragments, either directly at the metal (*e.g.* *via* reaction of $\text{H}_2\text{B}=\text{NH}_2$ with $[\text{Ir}(\text{PMe}_3)_2(\text{H})_2(\eta^2\text{-H}_2\text{B}=\text{NH}_2)]^+$, **I6a'**₇) or *via* an off-metal process^{43,42} involving two free aminoboranes. In fact for $\text{H}_3\text{B}\cdot\text{NH}_3$ both these processes are computed to be competitive with B–N coupling *via* **TS6a'**_{BN}, dimerisation at **I6a'**₇ having a transition state energy of +15.4 kcal mol⁻¹ while the off-metal process has a barrier of 16.2 kcal mol⁻¹ (see Fig. S16[†]). Some dimerisation (and trimerisation) may therefore be anticipated, and indeed evidence of this is seen in the small amount of borazine that is observed as minor products in the oligomerisation processes.

Overall the proposed dehydrogenation/oligomerisation mechanism captures the key trends observed experimentally by ESI-MS and NMR spectroscopy. In particular the promotional effect of added amine-borane on dehydrogenation for all three $\text{H}_3\text{B}\cdot\text{NMe}_x\text{H}_{3-x}$ ($x = 0–2$) species and the decreasing propensity toward oligomerisation as the size of the amine-borane increases are reproduced. However, some issues do remain: (i) the absolute barriers computed for the dehydrogenation are *ca.* 26 kcal mol⁻¹ and so are rather high for a (albeit slow) room temperature process; (ii) once dehydrogenation has occurred, the competing $\text{H}_2\text{B}=\text{NH}_2$ dimerisation processes are computed to be slightly more favourable than oligomerisation. One reason for these discrepancies may be the use of a model system in the present study, where PMe_3 is used in place of PCy_3 ligands. However, an additional factor may be that both the key N–H activation (*e.g.* **TS6a'**_{NH1}) and B–N coupling (*e.g.* **TS6a'**_{BN})



Scheme 5 Key steps in the oligomerisation of $\text{H}_3\text{B}\cdot\text{NH}_3$ at **I6a'**₁ in the presence of a third $\text{H}_3\text{B}\cdot\text{NH}_3$. Free energies (kcal mol⁻¹, BP86-D3(C₆H₅F)) are in kcal mol⁻¹.



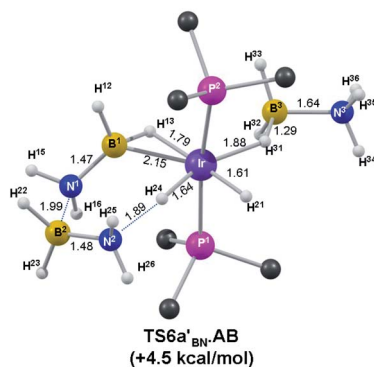


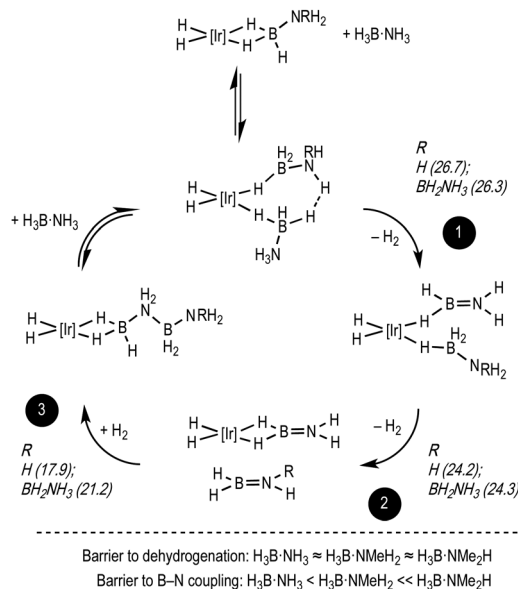
Fig. 7 Computed B–N coupling transition state in the presence of a third $\text{H}_3\text{B}\cdot\text{NH}_3$ molecule. Key distances in Å and PMe₃ H atoms omitted for clarity.

transition states exhibit a vacant site that offers the potential for further stabilisation. Indeed a third $\text{H}_3\text{B}\cdot\text{NH}_3$ molecule was found to promote both of these steps (see Scheme 5 and Fig. 7). Starting from **16a'**_{1,AB} dehydrogenation proceeds with a reduced overall barrier of 22.4 kcal mol⁻¹ to give **16a'**_{7,AB} at -4.9 kcal mol⁻¹ and from here B–N coupling has a barrier of only 9.4 kcal mol⁻¹. Moreover, B–N coupling (and the completion of the oligomerisation process) are now kinetically preferred over dimer formation. Therefore several substrate molecules may cooperate to promote the oligomerisation process. Alternatively a solvent molecule may interact with the unsaturated metal centre and so promote the oligomerisation step, although we have not attempted to explicitly model this here.

Conclusions

In summary, we report the observation and characterisation of multiple metal-bound oligomers in the dehydrocoupling of $\text{H}_3\text{B}\cdot\text{NH}_3$. This contrasts with only a single oligomerisation event being observed for $\text{H}_3\text{B}\cdot\text{NMe}_2\text{H}$ and none for $\text{H}_3\text{B}\cdot\text{NMe}_2\text{H}$. Interrogation of the likely mechanism using computational methods reveals that initial dehydrogenation of $\text{H}_3\text{B}\cdot\text{NH}_3$ is a higher energy process than both the subsequent dehydrogenation of a second amine-borane and metal-promoted B–N bond formation to form an oligomeric borazane bound to the metal centre. Steric factors play an important role in determining the barrier to B–N coupling which increases with x in the $\text{H}_3\text{B}\cdot\text{NMe}_x\text{H}_{3-x}$ series ($x = 0-2$). These studies also suggest a role for additional amine- or amino-borane in promoting dehydrocoupling processes through the formation of adduct species and complementary N–H...H–B interactions, an observation we noted from experimental studies both here and previously²¹ and recently from computational studies on related systems.⁴³

An overall mechanism that captures these observations is shown in Scheme 6. For $\text{H}_3\text{B}\cdot\text{NH}_3$ initial dehydrogenation of the amine-borane (step 1) has the highest barrier (+26.7 kcal mol⁻¹), with the subsequent dehydrogenation of a second amine-borane (step 2) proceeding through a slightly lower energy transition state at +24.2 kcal mol⁻¹. The transition state for the B–N coupling of the resultant amino-boranes (step 3) is then most



Scheme 6 Overall mechanism for the dehydrogenation and B–N bond forming events for $\text{H}_3\text{B}\cdot\text{NH}_3$. R = H (first oligomerisation, *i.e.* to form **6b**); R = BH_2NH_2 (second oligomerisation, **6c**). Numbers on parenthesis are calculated barriers for the model system (kcal mol⁻¹). $[\text{Ir}] = \{\text{Ir}(\text{PR}_3)_2\}^+$ (R = Cy, experiment; R = Me, computation).

accessible of all (+17.9 kcal mol⁻¹). The rather high barrier to dehydrogenation (step 1) means that these systems turnover rather slowly, especially compared to others that rapidly promote dehydrocoupling.⁶⁻¹² However, the corollary is that intermediates such as **6a-e** can be observed, allowing for direct mechanistic insight. For subsequent oligomerisations (*e.g.* to form **6c**, R = BH_2NH_3 Scheme 6) the key transition state energies retain the same pattern, thus promoting formation of a growing oligomeric chain at the metal centre. When the amine-borane is changed to $\text{H}_3\text{B}\cdot\text{NMe}_2\text{H}$ the same computed pattern still holds for the initial oligomerisation, but the second B–N coupling transition state (+24.8 kcal mol⁻¹) does become very close in energy to those for the two dehydrogenation steps (+25.4 kcal mol⁻¹ and +24.0 kcal mol⁻¹). Clearly B–N coupling is disfavoured by the greater bulk and experimentally only **5b** is observed to be formed. For $\text{H}_3\text{B}\cdot\text{NMe}_2\text{H}$ no B–N bond formation to give a linear diborazane is observed under these experimental conditions, with **4a*** formed only.

B–N coupling is also calculated to be competitive with amino-borane cyclisation, consistent with the observation of a small amount of borazine. However, coupling must be faster than reaction of exogenous cyclohexene with amino-borane as no hydroborated product is observed under these conditions. Our mechanism therefore has some similarities to those recently proposed for the catalytic dehydrocoupling of $\text{H}_3\text{B}\cdot\text{NH}_3$ using a bifunctional Ru-based catalyst¹⁰ and of $\text{H}_3\text{B}\cdot\text{NMe}_2\text{H}$ using $\text{Ir}(\text{tBuPOCOP}^t\text{Bu})\text{H}_2$.^{6,12} Although the intimate mechanistic details of these two systems likely differ, both propose dehydrogenation to form an amino-borane, that then must undergo fast metal-mediated B–N coupling, as neither system promotes hydroboration when exogenous cyclohexene is added.



Amine-borane dehydrocoupling presents a high degree of mechanistic complexity that is additionally highly catalyst specific. Although the precise mechanism outlined here might be rather system specific, the observations and suggested pathways presented might help guide future work on developing and understanding this challenging transformation. Ultimately the goal is the design of improved catalysts for this important process that have the potential to produce B-N materials “to order”.

Acknowledgements

The Rhodes Trust (A.K.), the University of Oxford, EPSRC (EP/J02127X/1) and the Spanish government (A.G.A.) for a Post-doctoral Fellowship (EX2009-0398).

Notes and references

- 1 E. M. Leitao, T. Jurca and I. Manners, *Nat. Chem.*, 2013, **5**, 817–829.
- 2 A. Staubitz, A. P. M. Robertson, M. E. Sloan and I. Manners, *Chem. Rev.*, 2010, **110**, 4023–4078.
- 3 Z. Liu, L. Song, S. Zhao, J. Huang, L. Ma, J. Zhang, J. Lou and P. M. Ajayan, *Nano Lett.*, 2011, **11**, 2032–2037.
- 4 B. L. Dietrich, K. I. Goldberg, D. M. Heinekey, T. Autrey and J. C. Linehan, *Inorg. Chem.*, 2008, **47**, 8583–8585.
- 5 A. Staubitz, A. Presa Soto and I. Manners, *Angew. Chem., Int. Ed.*, 2008, **47**, 6212–6215.
- 6 A. Staubitz, M. E. Sloan, A. P. M. Robertson, A. Friedrich, S. Schneider, P. J. Gates, J. S. auf der Günne and I. Manners, *J. Am. Chem. Soc.*, 2010, **132**, 13332–13345.
- 7 R. Dallanegra, A. P. M. Robertson, A. B. Chaplin, I. Manners and A. S. Weller, *Chem. Commun.*, 2011, **47**, 3763–3765.
- 8 J. R. Vance, A. P. M. Robertson, K. Lee and I. Manners, *Chem.–Eur. J.*, 2011, **17**, 4099–4103.
- 9 R. T. Baker, J. C. Gordon, C. W. Hamilton, N. J. Henson, P.-H. Lin, S. Maguire, M. Murugesu, B. L. Scott and N. C. Smythe, *J. Am. Chem. Soc.*, 2012, **134**, 5598–5609.
- 10 A. N. Marziale, A. Friedrich, I. Klopsch, M. Drees, V. R. Celinski, J. S. auf der Günne and S. Schneider, *J. Am. Chem. Soc.*, 2013, **135**, 13342–13355.
- 11 W. R. H. Wright, E. R. Berkeley, L. R. Alden, R. T. Baker and L. G. Sneddon, *Chem. Commun.*, 2011, **47**, 3177–3179.
- 12 A. P. M. Robertson, E. M. Leitao, T. Jurca, M. F. Haddow, H. Helten, G. C. Lloyd-Jones and I. Manners, *J. Am. Chem. Soc.*, 2013, **135**, 12670–12683.
- 13 T. Malakar, L. Roy and A. Paul, *Chem.–Eur. J.*, 2013, **19**, 5812–5817.
- 14 W. C. Ewing, A. Marchione, D. W. Himmelberger, P. J. Carroll and L. G. Sneddon, *J. Am. Chem. Soc.*, 2011, **133**, 17093–17099.
- 15 V. Pons, R. T. Baker, N. K. Szymczak, D. J. Heldebrant, J. C. Linehan, M. H. Matus, D. J. Grant and D. A. Dixon, *Chem. Commun.*, 2008, 6597–6599.
- 16 M. Käß, A. Friedrich, M. Drees and S. Schneider, *Angew. Chem., Int. Ed.*, 2009, **48**, 905–907.
- 17 H₂B=NMeH and H₂B=NH₂, or close derivatives thereof, have been trapped by coordination to a metal centre by dehydrogenation of the parent amine-borane. See, for example, G. Alcaraz, L. Vendier, E. Clot and S. Sabo-Etienne, *Angew. Chem., Int. Ed.*, 2010, **49**, 918–920; M. C. MacInnis, R. McDonald, M. J. Ferguson, S. Tobisch and L. Turculet, *J. Am. Chem. Soc.*, 2011, **133**, 13622–13633; M. A. Esteruelas, I. Fernández, A. M. López, M. Mora and E. Oñate, *Organometallics*, 2014, **33**, 1104–1107.
- 18 H. C. Johnson and A. S. Weller, *J. Organomet. Chem.*, 2012, **721–722**, 17–22.
- 19 C. J. Stevens, R. Dallanegra, A. B. Chaplin, A. S. Weller, S. A. Macgregor, B. Ward, D. McKay, G. Alcaraz and S. Sabo-Etienne, *Chem.–Eur. J.*, 2011, **17**, 3011–3020.
- 20 C. A. Jaska, K. Temple, A. J. Lough and I. Manners, *J. Am. Chem. Soc.*, 2003, **125**, 9424–9434.
- 21 H. C. Johnson, A. P. M. Robertson, A. B. Chaplin, L. J. Sewell, A. L. Thompson, M. F. Haddow, I. Manners and A. S. Weller, *J. Am. Chem. Soc.*, 2011, **133**, 11076–11079.
- 22 A. T. Lubben, J. S. McIndoe and A. S. Weller, *Organometallics*, 2008, **27**, 3303–3306.
- 23 L. P. E. Yunker, R. L. Stoddard and J. S. McIndoe, *J. Mass Spectrom.*, 2014, **49**, 1–8.
- 24 X. Yang and M. B. Hall, *J. Organomet. Chem.*, 2009, **694**, 2831–2838.
- 25 K. Ghatak and K. Vanka, *Comput. Theor. Chem.*, 2012, **992**, 18–29.
- 26 G. Bénac-Lestrille, U. Helmstedt, L. Vendier, G. Alcaraz, E. Clot and S. Sabo-Etienne, *Inorg. Chem.*, 2011, **50**, 11039–11045.
- 27 V. Butera, N. Russo and E. Sicilia, *Chem.–Eur. J.*, 2011, **17**, 14586–14592.
- 28 X. Chen, J.-C. Zhao and S. G. Shore, *J. Am. Chem. Soc.*, 2010, **132**, 10658–10659.
- 29 W. C. Ewing, P. J. Carroll and L. G. Sneddon, *Inorg. Chem.*, 2013, **52**, 10690–10697.
- 30 A. B. Chaplin and A. S. Weller, *Eur. J. Inorg. Chem.*, 2010, 5124–5128.
- 31 I. Koehne, T. J. Schmeier, E. A. Bielinski, C. J. Pan, P. O. Lagaditis, W. H. Bernskoetter, M. K. Takase, C. Würtele, N. Hazari and S. Schneider, *Inorg. Chem.*, 2014, **53**, 2133–2143.
- 32 L. S. Santos and J. O. Metzger, *Rapid Commun. Mass Spectrom.*, 2008, **22**, 898–904.
- 33 D. Guironnet, L. Caporaso, B. Neuwald, I. Göttker-Schnetmann, L. Cavallo and S. Mecking, *J. Am. Chem. Soc.*, 2010, **132**, 4418–4426.
- 34 ESI-MS has been used to analyse the metal-free product of dehydropolymerisation. See, for example, mass spectra reported in ref. 4, 6 and 12.
- 35 Calculations were run with the Gaussian suite of programs and employed the BP86 functional. Rh and P centres described with the Stuttgart RECPs and associated basis set with added d-orbital polarisation on P ($\zeta = 0.387$) and 6-31G** basis sets for all other atoms. Free energies are reported in the text, based the gas-phase values, incorporating corrections for dispersion effects using



- Grimme's D3 parameter set (*i.e.* BP86-D3) and solvent (C_6H_5F , PCM approach). See ESI† for references and full details.
- 36 R. Dallanegra, A. B. Chaplin and A. S. Weller, *Angew. Chem., Int. Ed.*, 2009, **48**, 6875–6878.
- 37 X. Chen, J.-C. Zhao and S. G. Shore, *Acc. Chem. Res.*, 2013, **46**, 2666–2675.
- 38 V. Butera, N. Russo and E. Sicilia, *ACS Catal.*, 2014, **4**, 1104–1113.
- 39 D. A. Addy, J. I. Bates, M. J. Kelly, I. M. Riddlestone and S. Aldridge, *Organometallics*, 2013, **32**, 1583–1586.
- 40 Experimentally, addition of sequential equivalents of $H_3B \cdot NMeH_2$ to **1** under a sparge of Ar to remove H_2 resulted in a reduced yield of **5b** with significant amounts of unidentified decomposition products formed.
- 41 When $H_3B \cdot NMe_2H$ is added to the amino-borane complex **4a*** significant (~35%) quantities of the corresponding linear diborazane are observed, suggesting that under these conditions of a high local concentration of $H_2B=NMe_2$ the B–N bond forming reaction is kinetically competent. See ref. 19. This experimental observation is consistent with the essentially similar barriers to dehydrogenation and B–N coupling calculated here for the secondary amine-borane. At lower concentrations of amine-borane used in this study dimerisation to form $[H_2B=NMe_2]_2$ dominates and the diborazane is not observed.
- 42 P. M. Zimmerman, A. Paul, Z. Zhang and C. B. Musgrave, *Inorg. Chem.*, 2009, **48**, 1069–1081.
- 43 L. J. Sewell, G. C. Lloyd-Jones and A. S. Weller, *J. Am. Chem. Soc.*, 2012, **134**, 3598–3610.

